Titanium Dioxide Structure Modified With Silver Chloride By 3D Printing For Dye Degradation And Bactericidal Applications

Po-Ching Lee
Tamkang University
Zheng-Rong Yang
Tamkang University
Chun-Yu Kuo
Tamkang University
Chung-Hao Shin
Tamkang University
Ching-Bin Lin (cblin@mail.tku.edu.tw)
Tamkang University

Research Article

Keywords: silver chloride, fused filament fabrication, azo dye, E. coli, reliability

Posted Date: March 11th, 2022

DOI: https://doi.org/10.21203/rs.3.rs-1421363/v1

Titanium dioxide structure modified with silver chloride by 3D printing for dye degradation and bactericidal applications

Po-Ching Lee[2] 、Zheng-Rong Yang[1] 、Chun-Yu Kuo[1] 、
Chung-Hao Shin[1] 、Ching-Bin Lin[1,] *

1 Department of Mechanical and Electro-Mechanical Engineering, Tamkang University, Tamsui, New Taipei, Taiwan, R.O.C.
2 Department of Water Resources and Environmental Engineering, Tamkang University, Tamsui, New Taipei, Taiwan, R.O.C.
*: Corresponding address: Department of Mechanical and Electro-Mechanical Engineering, Tamkang University, Tamsui, New Taipei, R.O.C.
Tel: +886-02-26215656 ext.2760
*: Corresponding author E-mail: cblin@mail.tku.edu.tw

Abstract

An advanced three-dimensional printing process for producing the Ag/AgCl/TiO_2-coupled photocatalyst was developed and tested for its stability and degradability in relation to azo dye (Orange II) and bacteria (*Escherichia coli*). The TiO_2 structure is produced through fused filament fabrication (FFF) with filaments of thermoplastic material, which is composed of TiO_2 anatase nanoparticles, high density polyethylene (HDPE), stearic acid, wax, and plasticizer. The TiO_2 structure is then solvent degreased, thermal degreased, and sintered to become a fundamental structure to couple the AgCl particles through an ion exchange process. Following the photoreduction of UV radiation, a Ag/AgCl/TiO_2-coupled photocatalyst is formed. In our experiments, this photocatalyst effectively degraded Orange II dye and sterilized *E. coli*. The degradation of Orange II dye and *E. coli* was performed under visible and ultraviolet light irradiation. The degradation kinetics of Orange II dye was a first-order reaction, with the degradability (94%) persisting for five cycles. The sterilization of *E. coli* was accomplished within 120 min, and the degradation kinetics were characteristic of a hyperbolic reaction. The photocatalytic module fabricated through FFF not only exhibited the ability to degrade contaminants in water but also exhibited durability and reliability after repeated use.

Key words: silver chloride; fused filament fabrication; azo dye; *E. coli*; reliability

1. Introduction

Thousands of chemicals are used in the textile dyeing industry, and the waste is a source of water contamination around the world. According to a World Bank report, approximately 17%–20% of industrial waste comes from the textile dyeing and finishing industries, and some of the ingredients are toxic to the environment, harming the environmental [1]. Of these, azo dye (Orange II) is environmentally persistent and

must be effectively treated before being released into a natural water body. Some of the disinfection processes that use chloride may generate by-products (e.g., trihalomethanes), which harm living creatures. Conventional treatment processes such as coagulation or biological processes may not efficiently remove or degrade these persistent chemicals sufficiently to meet drinking water standards. The use of photocatalysts as a medium for wastewater treatment is a chemical-free and safer method [2]. Examples include treatments with compounds such as TiO_2 photocatalyst, which generate free radicals that degrade dyes or disinfect germs efficiently [3]. The TiO_2 photocatalyst's 3.2-eV bandgap corresponds to light with a wavelength shorter than 380 nm in ultraviolet light. This wavelength range occupies only 5% of the band of solar radiation and limits the use of sunlight [4]. Some photocatalysts coupled with AgX (X = Cl, Br) might photoreduce the Ag atom cluster on the particle surface [5], causing surface plasmon resonance, which enhances the activity of the photocatalyst in the band range of visible light [6]. Kakuta et al. [7] compared the photocatalytic activity of Ag/AgCl and AgCl/N-doped TiO_2, concluding that Ag@AgCl material not only adsorbs the wavelength of UV light but also visible light, whereas AgCl/N-doped TiO_2 absorbs only UV light. Under visible light, the AgCl particle might photoreduce a few silver atom clusters and lower the bandgap to increase the usage rate of light [8-9]. Modification of the photolytic characteristics of TiO_2 by coupling metal or nonmetal compounds to broaden the absorption wavelength in the visible light range has been investigated [10-12], such as the coupling of TiO_2 with Ag/AgCl enhances the stability and capability of the photocatalyst used [13-17]. Although Ag/AgX (X=Cl/Br)/TiO_2-coupled photocatalytic particles in aqueous solution may improve photolytic efficiency and reduce costs, reusing technologies that challenge the collection or separation of nano-sized Ag/AgX (X = Cl/Br) particles coupled with a TiO_2 photocatalyst from the aqueous solution severely limits their application. Fixing the Ag/AgCl/TiO_2-coupled photocatalytic particles in a solid porous medium prevents them from being washed away. Our study used ceramic-fused filament fabrication (FFF) three-dimensional (3D) printing techniques to produce a highly specific surface area Ag/AgCl/TiO_2-coupled photocatalytic structure and test its durability and efficiency in degrading Orange II and disinfecting bacteria. When Ag/AgCl/TiO_2-coupled photocatalytic structure was placed in the medium, the prepared material derived its ability for activity enhancement from the surface plasmon resonance effect of the silver clusters, which enhanced the response of the material to visible light, effectively separating photogenerated electrons and holes. These electrons and holes can split water into high-activity free radicals such as hydroxyl (OH) and oxygen ion (O_2^-) [18]. Dyes that are widely used worldwide include nitroso, nitro, Orange II, sulfide, and indigoid dyes; Orange II is the most frequently used. According to Nilsson et al. [19], Orange II can be absorbed through

the skin and is potentially toxic and carcinogenic to humans. Silver chloride is a strong photocatalytic agent under sunlight and can degrade dyes effectively [20]. However, Ag@AgCl can also disinfect by killing bacteria, such as *Escherichia coli* and *Penicillium sp.* [21]. In addition, Ag/AgCl/TiO_2-coupled photocatalyst can kill *E. coli* and *Staphylococcus aureus* more effectively than the TiO_2 photocatalyst alone [22-23]. Materials coupled with the Ag/AgCl photocatalyst to enhance catalytic performance have been investigated recently, such as Ag/AgCl/WO_3 [24], Ag/AgCl/MCM-41 [25], Ag/AgCl/TiO_2 [26], Ag/AgI/Al_2O_3 [27], Ag/AgCl/ZnO [28], and AgCl/rGO [29]. These materials aim to shorten the bandgap of the photocatalytic energy and use a wide spectrum of visible light to improve the catalytic manifestation.

A few ceramic 3D printing techniques have been developed in this field, such as ceramic-filament fused fabrication (ceramic-FFF), binder jetting deposition, powder sintering deposition, paste extrusion deposition, selective laser sintering, direct ceramic ink-jet, and photopolymerization. Of these, FFF can be applied to create a porous or highly specific surface area structure. Using melt mixing and extruding PP/TiO_2 nanoparticle composite filaments and using the FFF process to fabricate nanocomposites, the mechanical properties increase with the increase of TiO_2 filler content, while the microstructural effects and processing properties of the materials are not significant [30]. PLA/antibacterial ceramic (ZnO and TiO_2) composite filaments exhibit thermal phase behavior and thermal stability suitable for 3D printing, and poly (ethylene glycol) plasticizers can be used to tune mechanical properties without affecting the antibacterial efficacy of ZnO and TiO_2 impregnation [31]. According to Vidakis et al. [32], they used acrylonitrile butadiene styrene (ATO, TiO_2) nanocomposite filaments and the FFF process to fabricate 3D printed structures. Appropriate ATO and TiO2 nanofiller content can increase the mechanical properties of 3D structures. By fused deposition modeling, TiO_2 -based photocatalytic filters were produced, and the PLA/30 wt% TiO_2 nanoparticle photocatalyst exhibited 100% methyl orange (MO) degradation after 24 h of illumination [33]. According to Sebastaki et al. [34], 100% recycled solid polystyrene was composited with 40% w/w TiO_2 nanoparticles to make composite filaments, which were then printed using an FDM process to fabricate 3D structures with photocatalysis. The ceramic-FFF process is similar to the Fused deposition modeling (FDM) process except that different materials are used. It uses a continuous filament of thermoplastic material, which is fed from a large filament through a moving heated print head and deposited on the growing surface of the printed shape. The print head is moved under programmable control to define the shape. The filament material used in ceramic FFF printing has ceramic particles added to the thermoplastic material (such as HDPE, PLA, ABS etc.) in conjunction with other ingredients including wax, steric acid and plasticizer. The filament material is

constantly heated and extruded by the printing head, layer by layer, to form the desired shape. After the 3D printing object is completed, the printed object (green compact) is removed the thermoplastic and organic ingredients then moved to a sintering furnace to form a solid concrete-like ceramic. The ceramic module is then immersed in a solution containing tin chloride and silver nitrate for ion exchange, resulting in AgCl/TiO_2-coupled photocatalyst. After the UV photoreduction reaction and drying process, a Ag/AgCl/TiO_2-coupled photocatalytic structure is made.

2. Experimental

2.1 Feedstock material for 3D printing

In FFF, the feedstock material extrusion is used for printing, during which a feedstock material is pushed through an extruder. In FFF machines, the feedstock material is in the form of a filament. In this experiment, the filament contained 20 nm of TiO_2 anatase nanoparticle powder (50 wt%), high-density polyethylene (HDPE, 40 wt%), wax (4.5 wt%), stearic acid (1.5 wt%), and plasticizer (4%). These materials were stirred in a Banbury mixer (Well Shyang Machinery, SBI-3L, Taiwan) at 50 rpm and 175 ^{o}C for 30 min to ensure all the ingredients were well melted and mixed. The mixture was then sliced and smeared to form a particle mixture for further melting, producing a thread-like filament. The filament was made by extrusion the particle mixture through a single screw extruder (Der-Hsin Plastic Machinery, Taiwan) with an inlet temperature of 160°C, a nozzle of 1.75 mm in diameter, and a 30-rpm rotating speed to produce a linear thread with a diameter of 1.70–1.80 mm and ellipticity of 0.1 mm (where 0 indicates a true circle).

2.2 Ceramic fused-thread 3D printing head, module design, and manufacturing

The Ag/AgCl/TiO_2-coupled photocatalytic module included a highly specific surface area Ag/AgCl/TiO_2-coupled photocatalytic cylinder and a set of upper and lower pressure polylactic acid (PLA) plates, in which an internal thread was machined in a circular hole in the upper and lower pressure plates to form a screw connection with a male thread in the rotating shaft. The size specifications are presented in Figure 1. The highly specific surface area Ag/AgCl/TiO_2-coupled photocatalytic cylinder was adapted for structural strength and flow-field design. The manufacturing process of the highly specific surface area Ag/AgCl/TiO_2-coupled photocatalytic module proceeds as follows. First, the stirring rotating shaft is passed through the highly specific surface area AgCl/TiO_2-coupled photocatalytic cylinder, the internal thread is screwed into the circular hole in the lower PLA plate, and then the upper PLA plate is placed in the stirring shaft on the upper surface of the highly specific surface area AgCl/TiO_2-coupled photocatalytic cylinder. Bolts are used to spin the upper surface of the photocatalyst cylinder for the upper PLA plate to be combined tightly with the AgCl/TiO_2-coupled photocatalytic cylinder. Finally, near-ultraviolet light is irradiated

to generate photoreduction to prepare a highly specific surface area Ag/AgCl/TiO_2-coupled photocatalytic module.

2.3 3D printing of the TiO_2 photocatalytic cylinder

A self-made FFF 3D printer was used to print the highly specific surface area TiO_2 photocatalyst cylinder. Commercial slicing software was used to set the printing parameters and generate G-codes for the printing devices based on 3D-CAD models. The printer had a print head speed of 10 mm/sec, print bed temperature of 80°C, print layer height of 0.2 mm, bronze nozzle of 0.4 mm, nozzle temperature of 200°C, oversizing factor (x, y) of 19.87%, oversizing factor (z) of 25.32%, and infill of 30%. Fused filament fabrication was performed on a 304 stainless steel substrate at 80°C, with a positioning system that had a spatial resolution with a *z*-axis of approximately 100 μm, and the spatial resolution of the *x*-axis and *y*-axis was approximately 11 μm. Because of the brittle nature of the 3D printing wire, the entire fused filament fabrication deposition printing system was maintained at 50°C to increase its ductility. The printed object (green compact) was immersed in *n*-hexane at 60°C for 2 h to dissolve the wax and open the pores. The HDPE retained the shape of the green compact, which was then thermally degreased at 350°C for 85 min and 500°C for 1 h to remove any residual organic matter. Figure 2(a) depicts the formation of a dense TiO_2 photocatalyst cylinder in a high-temperature furnace at 10^{-1} bar and 1200°C for 0.5 hours.

2.4 Manufacture of the Ag/AgCl/TiO_2-coupled photocatalytic structure

We used an ion exchange method to prepare the Ag/AgCl/TiO_2-coupled photocatalytic structure (Figure 3). First, we immersed the sintered TiO_2 photocatalyst cylinder into a solution containing 30 mmol of $SnCl_2 \cdot 2H_2O$, 1.5 mL of HCl (35%), and 30 mL of deionized water. After 30 min of sensitized reaction in the solution, the cylinder was washed with deionized water several times to remove any residual chemicals from the surface. The sensitized TiO_2-coupled photocatalytic cylinder was then placed in 20 mL of 5 mmol $AgNO_3$ deionized aqueous solution for 30 min for the activation reaction and then washed with deionized water several times to remove any residual chemicals from the surface. The AgCl/TiO_2-coupled photocatalytic cylinder was then dried at 100 ℃ for 2 hours and UV irradiated to produce photoreduction. Finally, a photocatalytic cylinder coupled with Ag/AgCl/TiO_2 was prepared, and the cylinder was assembled with the upper and lower pressure plates and the stirring shaft to complete the module [Figure 2(b)]. The X-ray diffractometer (BRUKER, D8A) which was operated at incident light with wavelength 1.54056 Å (CuKα) by copper target, scanning angle 2θ from 10° to 90°, a scanning rate of 0.1° s^{-1}, was used to compare and analyze the phases of crystalline phase of the sintered-TiO_2 and the Ag/AgCl/TiO_2-coupled photocatalyst [Joint Committee on Powder Diffraction Standards (JCPDS): 87e0597), AgCl (JCPDS:

85e1355), and anatase-phase TiO_2 (JCPDS: 71e1166).

2.5 Degradation of Orange II through Ag/AgCl/TiO_2-coupled photocatalytic module

The photocatalytic characteristics of the prepared Ag/AgCl/TiO_2-coupled photocatalytic module were studied through the degradation of Orange II. Orange II was dissolved in deionized water to a concentration of 30 ppm. UV light (365 nm) output at 9 W and visible light (435, 545, and 612 nm) output at 9 W were used as the light sources. Figures 4(a) and (b) present the UV and visible light spectrums, respectively. Both ultraviolet (365 nm) and visible light (435, 542, and 612 nm) were used because the Ag/AgCl/TiO_2-coupled photocatalyst absorbs ultraviolet rays and decomposed water to produce a substantial amount of highly active •OH and $\bullet O_2^-$ for photocatalysis. Three blank tests were applied to check the photocatalytic ability without a photolytic module, light sources, or both, for comparison. The Ag/AgCl/TiO_2-coupled photocatalytic module was setup and tested as follows. A 500-mL glass beaker was used as the reactor and placed on a thermostat to maintain it at 25°C. In each test, the dye solution had a concentration of 30 ppm and was mixed through constant stirring. The Ag/AgCl/TiO_2-coupled photocatalyst was hung in the dye solution, and a water lever was placed just above the photocatalysts. Both UV and visible light were placed near the glass beaker, as illustrated in Figure 5(a). After the experiment had begun and the light source was irradiated, samples were taken periodically to analyze the degradation rate of the Orange II solution. The concentration of Orange II that had been degraded was measured following the standard National Institute of Environmental Analysis method, W223.50B, in which the absorbance of the solution is measured at different wavelengths using a spectrophotometer and the American Dye Manufacturers Institute (ADMI) value is calculated.

2.6 Disinfection of *E. coli* using the Ag/AgCl/TiO_2-coupled photocatalyst module

The ability to disinfect *E. coli* using the Ag/AgCl/TiO_2-coupled photocatalytic module was tested in a similar manner to that of the degradation of Orange II, with *E. coli* used as the test medium. The *E. coli* sample was prepared by cultivating *E. coli* in a liquid nutrient (lysogeny) broth to a concentration of 0.6–0.8 M at an optical density of 600 nm. The photocatalytic reaction then occurred in the Ag/AgCl/TiO_2-coupled photocatalyst module under UV (9 W; 365 nm) and visible (9 W; 435, 545, and 612 nm) light conditions for predetermined durations. The experimental setup for the photocatalytic disinfection of *E. coli* is depicted in Figure 5(b). The number of bacteria was determined through the establishment of the colony forming number (colony forming unit) by 1) diluting the samples (known dilution ratio), 2) removing 100 μL of the diluted solution, and 3) smearing the samples on a nutrient agar Petri dish for a 24-h incubation period (37°C). The bacteria colony then grew, and the number of bacteria

in the Petri dish was counted. Each set of the experiment was triple sampled within a predetermined period, cultivated, and counted for accuracy. Blank tests were also conducted for accuracy.

3 Results and discussion

3.1 Characteristics of the 3D printing filament

The microstructure of the sintered-TiO_2 and Ag/AgCl/TiO_2–coupled photocatalyst are presented in Figure 6(a) and (b), respectively. AgCl particles with an average diameter of 20 nm were scattered on the surface of the filament, and the presence of Ag on the AgCl surface was identified through energy dispersive spectroscopy (EDS) and a mapping analysis [Figure 6 (c) and (d)]. The mechanisms underlying the coupling of the AgCl particles with the sintered-TiO_2 are presented in Figure 3. The sintered-TiO_2 photolytic cylinder was exposed to a solution containing $SnCl_2 \cdot 2H_2O$ and 35% HCl for sensitization, and the ionic Sn^{2+} and Cl^- may adsorb to the surface of the sintered-TiO_2 photolytic cylinder. Applying the $AgNO_3$ solution to the cylinder with the Ag^+ and Cl^- forms AgCl particles on the sintered-TiO_2 photolytic cylinder. After passing through the UV light radiation, the photoreduction reaction occurs and the coupled Ag/AgCl/TiO_2 photocatalyst is formed. The analytical results of X-ray diffraction related to the formed material are presented in Figure 7. According to the JCPDS database, the diffraction angle and Miller indices of crystal TiO_2 are 25° (101), 38° (004), 48° (200), 54° (105), and 55° (201). The diffraction angle and Miller indices of crystal AgCl are 28° (111), 32° (200), and 46° (220). The reduced form of the Ag cluster was 38° (111), a value that fit the data from the crystal Ag/AgCl well.

3.2 Degradation of Orange II

In the blank 140-min test without light irradiation (only use the Ag/AgCl/TiO_2–coupled photocatalytic module), the results indicated less than 2% degradability, suggesting that the photocatalyst was photocatalyzed and activated only under light conditions. The relationship between time scales and different types of Orange II concentrations is depicted in Figure 8(a)–(c). In the figure, C represents the concentration of Orange II at time t and C_0 is the initial concentration of 30 mg/L. In this study, the reaction rate was consistent with first-order (or pseudo-first-order) kinetics [35], in which the quantity $ln(C/C_0) = k_{app} \times t$ can serve as an indicator of performance. In the preceding equation, k_{app} is the apparent rate constant that indicates the degradability of the photocatalyst. The value of k_{app} for Orange II degradation was 0.02 min^{-1}. Furthermore, C/C_0 is defined as follows:

$C/C_0 = 1 - t / (a + bt)$ or $t / [1 - (C/C_0)] = a + bt$,

where a and b are constants related to catalyst properties. The hyperbolic relations are presented in Figure 8(b), and the values of a and b and of the correlation coefficient(R^2) were 33.71, 0.866, and 0.99, respectively. The large correlation coefficient (0.99)

indicated that the tests performed were more likely to accord with the hyperbolic kinetics relations than pseudo-first-order kinetics.

The mechanisms underlying the degradation of Orange II dye (Figure 9) may be related to the powerful oxidative free radicals, such as $\bullet O_2^-$, which are generated through the process, in which electrons (e^-) interact with O_2 atoms on the surface of the AgCl. The electron hole (h^+) may react with OH^- to produce an OH^- free radical. Both $\bullet O_2^-$ and $\bullet OH^-$ are strong oxidants and could break down the organic compound Orange II into CO_2 and water. Additionally, some electron holes may react with AgCl to produce Ag^+ and Cl^0, wherein Ag^+ accepts electrons from the conduction band and forms Ag atoms and clusters, preventing the further catalysis of AgCl. Cl^0 is also a strong oxidant that breaks down Orange II dye and forms CO_2, H_2O, and Cl^-. The surface plasmon resonance reaction of the Ag cluster on AgCl may absorb visible light intensively, thus leading to the increased production of Ag^+ and e^-, with some Ag^+ and Cl^- materials combining to reform AgCl. Additional, most of the electrons can flow from TiO_2 to AgCl to Ag clusters, mainly because the Fermi level of TiO_2 (4.89 eV) is higher than that of AgCl (4.6 eV) and Ag clusters (4.28 eV). Therefore, Ag clusters have too many electrons, while TiO_2 has too many holes, so the recombination of electrons and holes of Ag/TiO_2 can be prevented, which is beneficial to improve the performance of the photocatalyst. This phenomenon results in a highly stable and repeatable condition under which the reuse of this photocatalyst is feasible. Under UV and visible light conditions with five cycles of reuse, when the $Ag/AgCl/TiO_2$–coupled photocatalyst (cleaned with distilled water and air-dried before each use) was used, the degradability remained at 94%, as illustrated in Figure 10. This module therefore has high stability and durability.

3.3 Disinfection of *E. coli*

Photographs of the disinfection process using the $Ag/AgCl/TiO_2$–coupled photocatalyst are presented in Figure 11, and Figure 12 presents the relationship between the time scales and colony numbers of different types of *E. coli*.

$C/C_0 = 1 - t / (a + bt)$ or $t / [1 - (C/C_0)] = a + bt$,

where a and b are constants related to catalyst properties. The hyperbolic relations are presented in Figure 12(a), and the values of a and b and of the correlation coefficient (R^2) are 2.415, 0.988, and 0.9998, respectively. The disinfection efficiency is provided as a percentage in Figure 12(b). The mechanisms behind *E. coli* disinfection may be related to the generation of Ag atoms or free radicals when UV or visible light photons hit the photocatalyst. When the Ag atoms interact with *E. coli*, some phosphoryl amino acids (e.g., phosphoryl tyrosine) are dephosphorylated and the original function of the protein is altered or stopped, which, in turn, slows the growth of *E. coli*. The produced free radicals act as strong oxidants that could break the cell wall and cause the leakage

of essential materials, such as proteins, glucose, and K ions, from the cytoplasm to the external environment. The cell membrane potential, the consumption of adenosine triphosphate, or the permeability of the cell membrane could then be seriously compromised to the point of malfunction or death. Ag nanoparticles may penetrate the cell membrane and combine with the thiol group of some enzymes (e.g., dehydrogenase) in cells to stop the function of these enzymes, which, in turn, deactivates the basic metabolism of that cell. In a moist environment, Ag^+ and electrons may be released from Ag clusters and react with the O_2 in water, thus producing $\bullet O_2^-$, H_2O, or •OH. These are all strong free radicals and could effectively deactivate the metabolism of most cells. When Ag^+ interacts with bacteria, it may combine with the sulfhydryl group (–SH) in proteins, and the original disulfide bond (–S–S–) is broken into a denatured status (–SAg). The Ag^+ eventually stops the reactions in cell respiration or electron transport, causing cell mortality. After cell destruction, Ag^+ is released, destroying more cells. This process helps the employed photocatalyst to repeatedly and effectively disinfect the bacteria. The blank test (without light radiation) exerted no observed effect on *E. coli* growth, which indicates that photons play a role in activating the reaction [36-37].

4 Conclusions

In the present study, we fabricated the Ag/AgCl/TiO_2–coupled photocatalyst through the 3D printing of ceramic fused filament fabrication. The Ag/AgCl/TiO_2–coupled photocatalytic module was investigated for its ability to degrade Orange II dye and kill *E. coli* under UV and visible light conditions. This module was appropriate for degrading dyes and bacteria within minutes and hours, respectively, with the degradability remaining high (94%) after five cycles of reuse. The application of the Ag/AgCl/TiO_2–coupled photocatalytic module as a photocatalyst for contaminant degradation is promising, as indicated by the effectiveness, reliability, and structural durability it demonstrated in this study.

Acknowledgements

This study was supported by the Ministry of Science and Technology of the Republic of China, Taiwan (MOST 109－2221－E－032－021－)

Ethics declarations

Conflict of interest

No conflict of interest exits in the submission of this manuscript, and the manuscript is approved by all authors for publication. I would like to declare on behalf of my co-authors that the work described was original research that has not been published previously, and not under consideration for publication elsewhere in whole or in part. All the authors listed have approved the manuscript that is enclosed.

6.Reference

1.Huang S T, Jiang Y R, Chou S Y, Dai Y M, Chen C C, Synthesis, characterization, photocatalytic activity of visible-light-responsive photocatalysts BiO_xCl_y/BiO_mBr_n by controlled hydrothermal method. J. Mol. Catal. A: Chem.,**391(1)**,105(2014).

2.Low J, Yu J, Jaroniec M, Wageh S, Al-Ghandi A A., Heterojunction Photocatalysts, Adv. Mater. ,**29(20)**,1601694(2017).

3.Fujisima A, Hinda K., Electrochemical Photolysis of Water at a Semiconductor Electrode., Nature, **238**,37(1972).

4.Libanori R, Giraldi T R, Longo E, Leite E R, Effect of TiO_2 surface modification in Rhodamine B photodegradation, J. Sol. Gel. Sci. Technol., **49(1)**,95(2009).

5.Choi M, Shin K H, Jang J, Plasmonic photocatalytic system using silver chloride/silver nanostructures under visible light, J. Colloid Interface Sci., **341(1)**, 83(2010).

6.Wang H, Gao J, Guo T, Wang R, Li J, Facile Synthesis of AgBr Nanoplates with Exposed {111} Facets and Enhanced Photocatalytic Properties. Chem. Commun., **48**,275(2012).

7.Kakuta N, Goto N, Ohkita H, Mizushima T, Silver Bromide as a Photocatalyst for Hydrogen Generation from CH_3OH/H_2O Solution, J. Phys. Chem. B, **103(29)**,5917(1999).

8.Wang P, Huang B, Qin X, Zhang X, Dai Y, Wei J, M. Whangbo M, Ag@AgCl: A Highly Efficient and Stable Photocatalyst Active under Visible Light†. Angew. Chem. Int. Ed.,**47**,7931(2008).

9.Wang Y, Wang Q, Zhan X, Wang F, Safdar M, He J, Visible light driven type II heterostructures and their enhanced photocatalysis properties: a review., Nanoscale,**5**,8326(2013).

10.Zielińska-Jurek A, Wei Z, Wysocka I, Szweda P, Kowalska E, The effect of nanoparticles size on photocatalytic and antimicrobial properties of Ag-Pt/TiO_2 photocatalysts, Appl. Surf. Sci., **353**,317(2015).

11.Liu T, Liu B, Yang L, Ma X, Li H, Yin S, Sato T, Sekino T, Wang Y, RGO/Ag_2S/TiO_2 ternary heterojunctions with highly enhanced UV-NIR photocatalytic activity and stability, Appl. Catal. B Environ., **204**,593(2017).

12.Farsinezhad, Samira; Banerjee, Shyama Prasad; Bangalore Rajeeva, Bharath; Wiltshire, Benjamin D.; Sharma, Himani; Sura, Anton; Mohammadpour, Arash; Kar, Piyush; Fedosejevs, Robert; Shankar, Karthik, Reduced Ensemble Plasmon Line Widths and Enhanced Two-Photon Luminescence in Anodically Formed High Surface Area Au–TiO_2 3D Nanocomposites, ACS Appl. Mater. Interfaces, **9(1)**,740(2016).

13.Zhang J, Liu X, Suo X, Li P, Liu B, Shi H, Facile synthesis of Ag/AgCl/TiO_2 plasmonic photocatalyst with efficiently antibacterial activity, Mater. Lett.,

198,164(2017).
14.Liu W, Chen D, Yoo S, Cho S, Hierarchical visible-light-response Ag/AgCl@TiO_2 plasmonic photocatalysts for organic dye degradation, Nanotechnology, 24(40),405706(2013). 15.Shah Z, Wang J S, Ge X, Wang C, Mao W, Zhang. S, Highly enhanced plasmonic photocatalytic activity of Ag/AgCl/TiO_2 by CuO co-catalyst, J. Mater. Chem. A, **3(7)**,3568(2015).
16.Ge Z, Ji Y, Qiu Y, Chong X, Feng J, He J, Enhanced thermoelectric properties of bismuth telluride bulk achieved by telluride-spilling during the spark plasma sintering process, Scripta. Mater., **143**,90(2018).
17.Yang L, Ma X, Zhang W, Gen W, Ag@AgCl-TiO_2/organic rectorite/quaternized chitosan microspheres: An efficient and environmental photocatalyst. J. Appl. Polym. Sci. **134**,44601(2016).
18.Tang B, Zhang Q, Characterization of Photocatalysis of AgCl Colloid, J. Univ. Sci. Technol. China, **32(6)**,743(2002).
19. Nilsson, R., R. Nordlinder, U. Wass, B. Meding and L. Belin, Asthma, Rhinitis, and dermatitis in workers exposed to reactive dyes, British Journal of Industrial Medicine, **50**,65(1993).
20.Song C, Zhang Q, Tang B, On the photocatalytic degradation of pigment by AgCl film, J. Anhui Inst. Mech. Electr. Eng., **18(1)**,23(2003).
21.Zhang Q, Tang B, Preparation of Colloid Antibacterial AgCl Film and Its Antibacterial Characterization under Photo Catalysis, J. Nanjing Univ. Sci. Technol. Nat. Sci. ,**28(5)**,547(2004).
22.Christensen P A, Curtis T P, Egerton T A, Kos S A M, Tinlin J R, Photoelectrocatalytic and photocatalytic disinfection of E. coli suspensions by titanium dioxide, Appl. Catal. B, **41(4)**,371(2003).
23.Sikong L, Noophum B, Kooptarnond K, Photodegradation of Contaminants and Antibacterial Activity Enhanced by AgCl Nanoparticles on N, S, Co-Doped TiO_2 Thin Films, Dig. J. Nanomater. Bios., **10(2)**,455(2015).
24.Guo J F, Ma B W, Yin A Y, Fan K N, Dai W L, Highly stable and efficient Ag/AgCl@TiO_2 photocatalyst: Preparation, characterization, and application in the treatment of aqueous hazardous pollutants, J. Hazard. Mater.,**211-212**,77 (2012).
25.Sohrabnezhad S, Pourahmad A, As-synthesis of nanostructure AgCl/Ag/MCM-41 composite, Spectrochim. Acta A Mol. Biomol. Spectrosc., **86**,271 (2012).
26.Yang Q, Hu M, Guo J, Ge Z, Feng J, Synthesis and enhanced photocatalytic performance of Ag/AgCl/TiO_2 nanocomposites prepared by ion exchange method, J. Materiomics, **4(4)**,402(2018).
27.Hu C, Peng T W, Hu X X, Nie Y L, Zhou X F, Qu J H, He H, Plasmon-Induced Photodegradation of Toxic Pollutants with Ag−AgI/Al_2O_3 under Visible-Light

Irradiation, J. Am. Chem. Soc., **132(2)**,857(2010).
28.Xu Y G, Xu H, Li H M, Xia J X, Liu C T, Liu L, Enhanced photocatalytic activity of new photocatalyst Ag/AgCl/ZnO, J. Alloys Compd.,**509(7)**,3286(2011).
29.Luo G Q, Jiang X J, Li M J, Shen Q, Zhang L M, Yu H G, Facile Fabrication and Enhanced Photocatalytic Performance of Ag/AgCl/rGO Heterostructure Photocatalyst, ACS Appl. Mater. Interfaces, **5(6)**,2161(2013).
30.Nectarios Vidakis, Markos Petousis, Emmanouil Velidakis, Lazaros Tzounis, Nikolaos Mountakis, John Kechagias and Sotirios Grammatikos, Optimization of the Filler Concentration on Fused Filament Fabrication 3D Printed Polypropylene with Titanium Dioxide Nanocomposites. Materials. **14(11)**,3076(2021).
31. Zachary Brounstein, Chris M. Yeager and Andrea Labouriau Development of Antimicrobial PLA Composites for Fused Filament Fabrication. Polymers. **13(4)**,580 (2021).
32.Nectarios Vidakis, Markos Petousis, Athena Maniadi, Emmanuel Koudoumas, Marco Liebscher and Lazaros Tzounis, Mechanical Properties of 3D-Printed Acrylonitrile–Butadiene–Styrene TiO2 and ATO Nanocomposites. Polymers. **12(7)**, 1589(2020).
33. A. Sangiorgi, Z. Gonzalez, A. Ferrandez-Montero, J. Yus, A. J. Sanchez-Herencia, C. Galassi, A. Sanson and B. Ferrari, 3D Printing of Photocatalytic Filters Using a Biopolymer to Immobilize TiO2 Nanoparticles. Journal of The Electrochemical Society.**166(5)**,H3239(2019).
34. Maria Sevastaki ,Mirela Petruta Suchea and George Kenanakis, 3D Printed Fully Recycled TiO2-Polystyrene Nanocomposite Photocatalysts for Use against Drug Residues.Nanomaterials.**10(11)**,2144(2020).
35.Saien J, Khezrianjoo S, Degradation of the fungicide carbendazim in aqueous solutions with UV/TiO_2 process: Optimization, kinetics and toxicity studies, J. Hazard. Mater., **157(2-3)**,269(2008).
36.Wang D, Li Y, Puma G L, Wang C, Wang P, Zhanga W, Wang Q, Mechanism and experimental study on the photocatalytic performance of Ag/AgCl @ chiral TiO_2 nanofibers photocatalyst: The impact of wastewater components, J. Hazard. Mater., **285**,277(2015)
37.Nie L, Hu B, Jiang J, Preparation of Ag/AgCl/TiO_2-XCX Plasmonic Photo-Catalyst with Enhanced Visible-Light Photocatalytic Activity, Adv. Mater. Res., 356-**360**,506(2012).

Figure Captions

Fig. 1(a) and (b) Design of the Ag/AgCl/TiO_2-coupled photocatalyst; (b) three-dimensional diagram of the Ag/AgCl/TiO_2 photocatalyst module.

Fig. 2(a) Structure of sintered-TiO_2 green compact completed using fused deposition printing; (b) Ag/AgCl/TiO_2-coupled photocatalytic module.

Fig. 3 Schematic of ion exchange method to prepare the Ag/AgCl/TiO_2-coupled photocatalyst.

Fig. 4 Light source spectrum of (a) UV light and (b) visible light.

Fig. 5 Setup for (a) degradation of azo dye (Orange II) and (b) disinfection of *E. coli*

Fig. 6 Microstructure of (a) sintered-TiO_2 and (b) Ag/AgCl/TiO_2-coupled photocatalyst Ti, O, Cl, and Ag identified using (c) energy dispersive spectroscopy and (d) mapping analysis

Fig. 7 X-ray diffraction pattern of (a) sintered-TiO_2 and (b) Ag/AgCl/TiO_2-coupled photocatalyst.

Fig. 8 Degradability of Orange II dye performed on different scales. (a) Concentration variation over time; (b) concentration logarithm in relation to initial concentration over time; (c) degradation over time (residual concentration to initial concentration).

Fig. 9 Mechanisms of Ag/AgCl/TiO_2 -coupled photocatalytic reaction.

Fig. 10 Degradation performance during five consecutive uses of the FFF module

Fig. 11 *E. coli* colony samples on a Petri dish after 15, 45, 75, 105, and 135 min of catalytic disinfection treatment.

Fig. 12 Degradability of *E. coli* performed at different scales. (a) Concentration variation over time; (b) degradability over time (residual concentration to initial concentration).

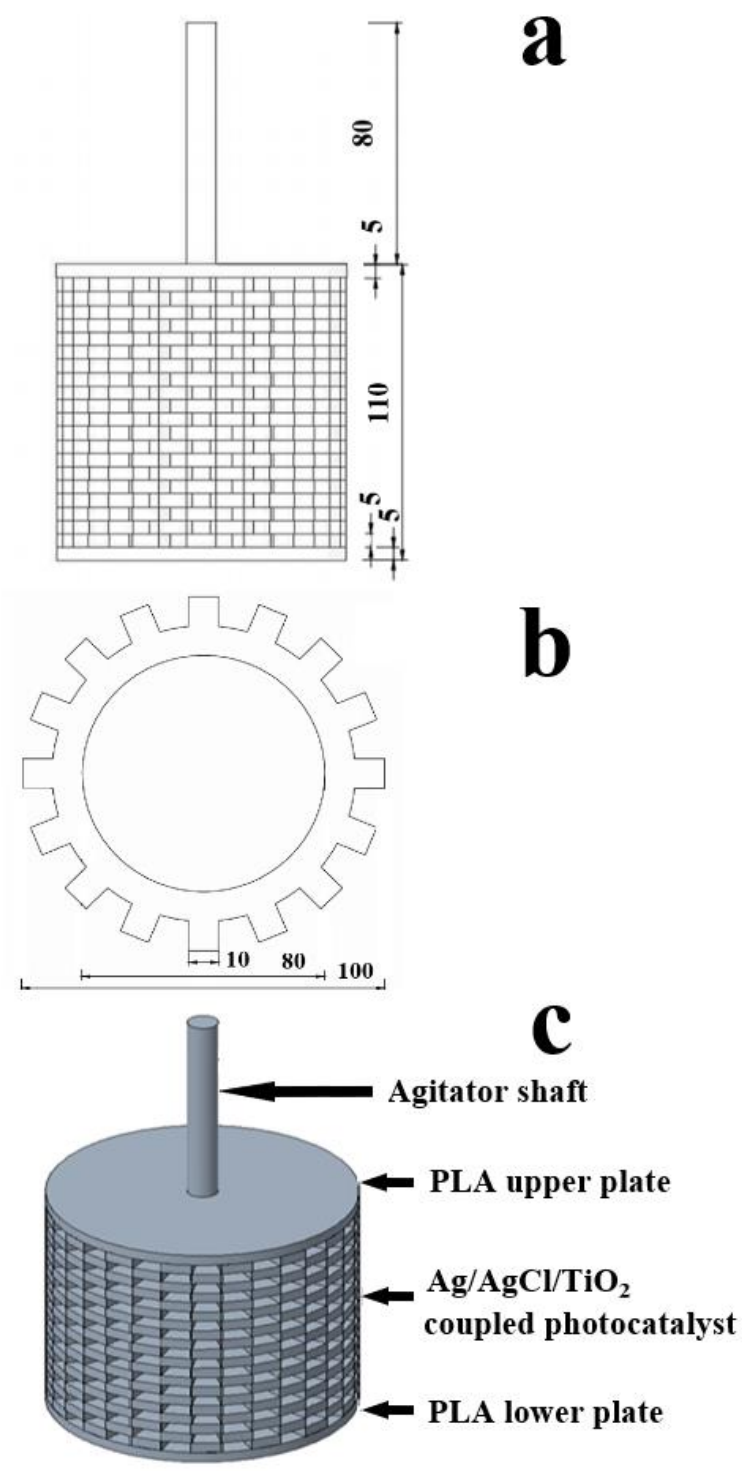

Fig.1-C.B. Lin et al.

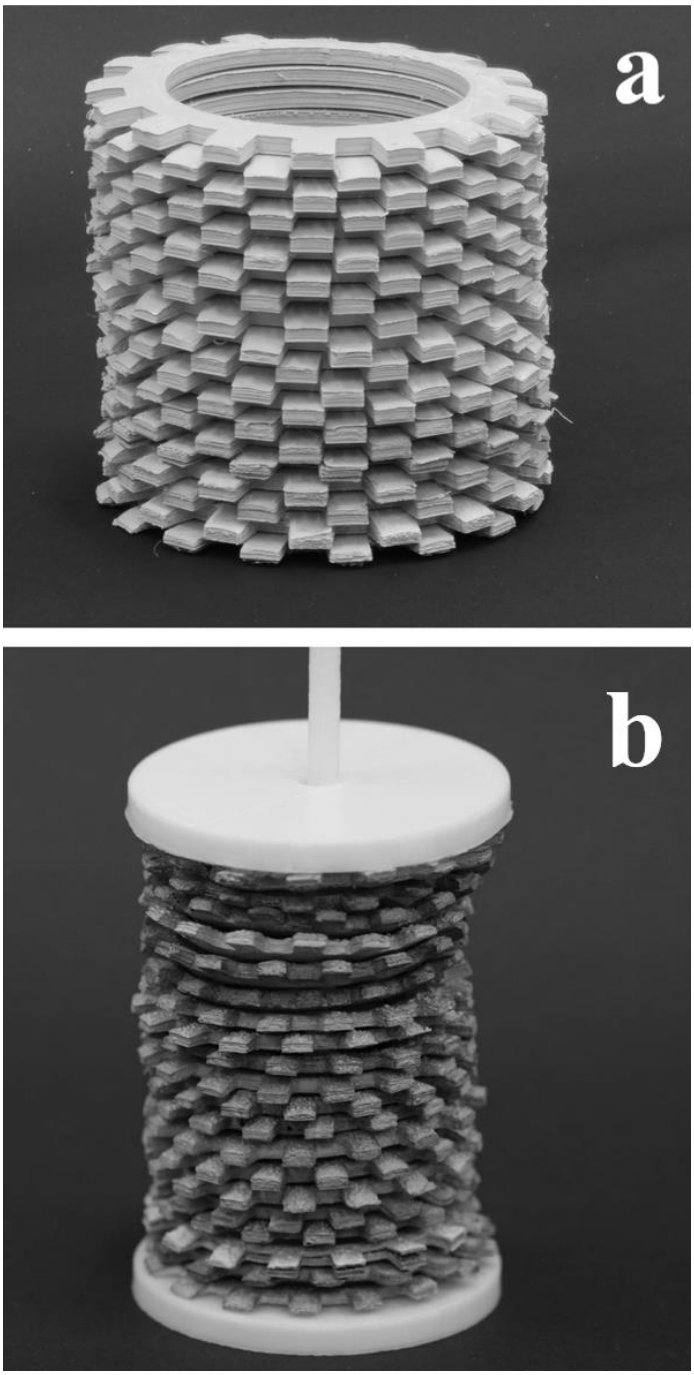

Fig.2-C.B. Lin et al.

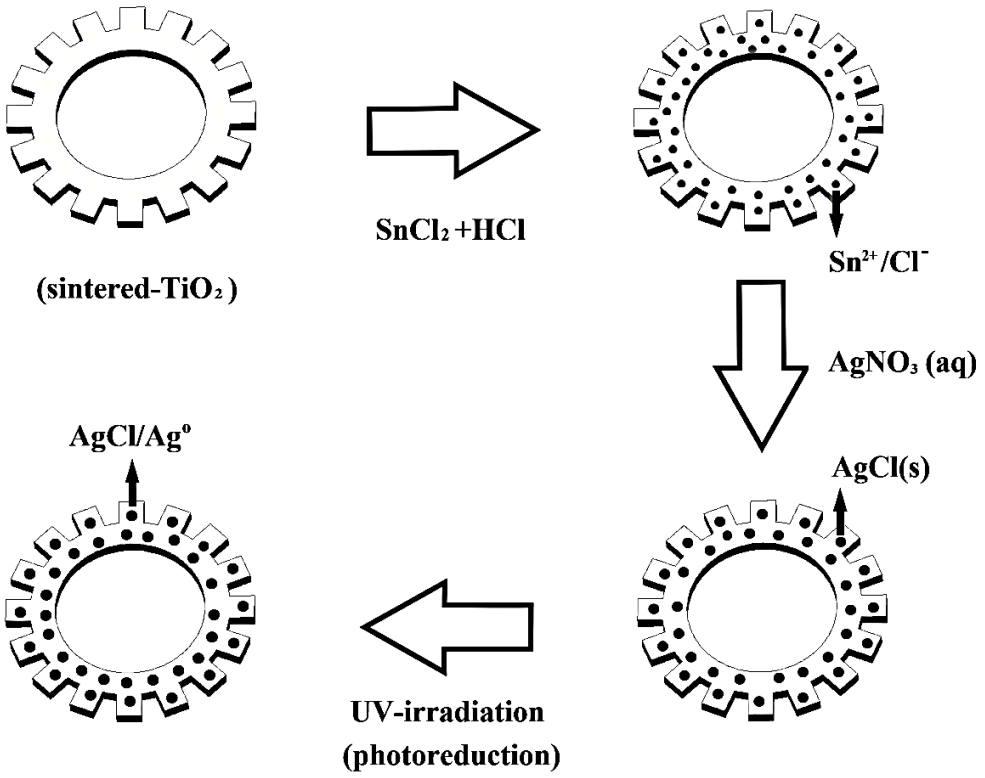

Fig.3-C.B. Lin et al.

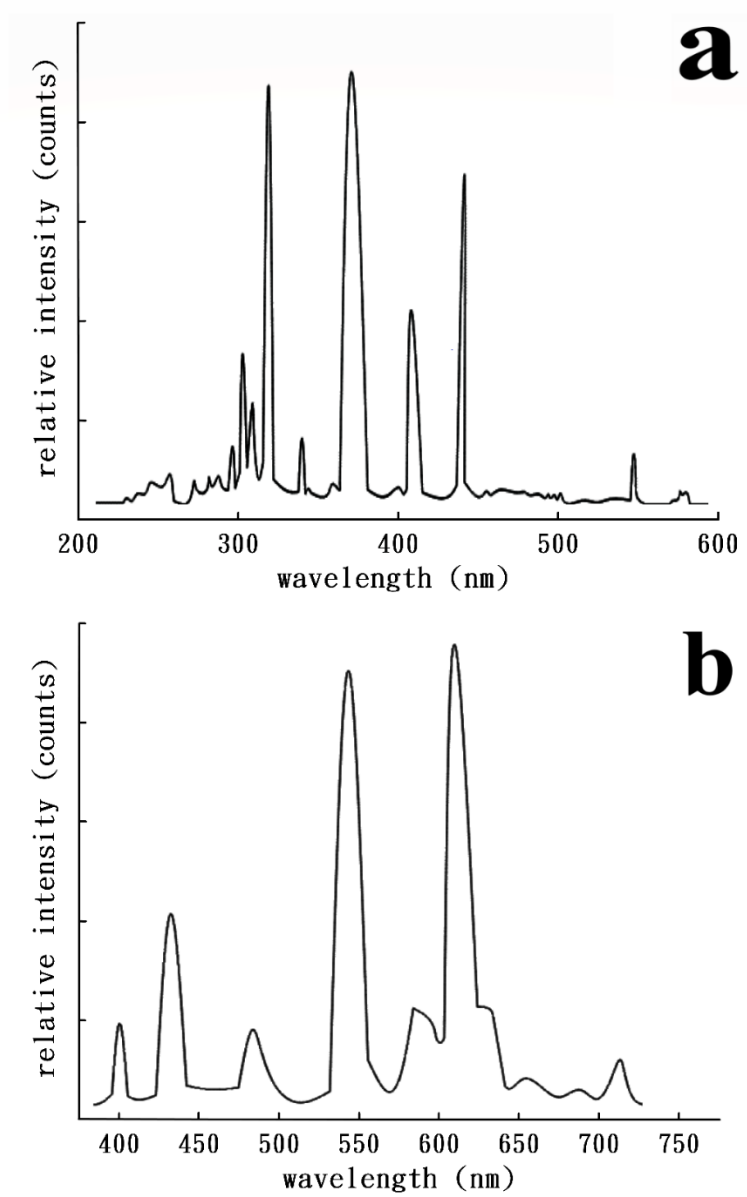

Fig.4-C.B. Lin et al.

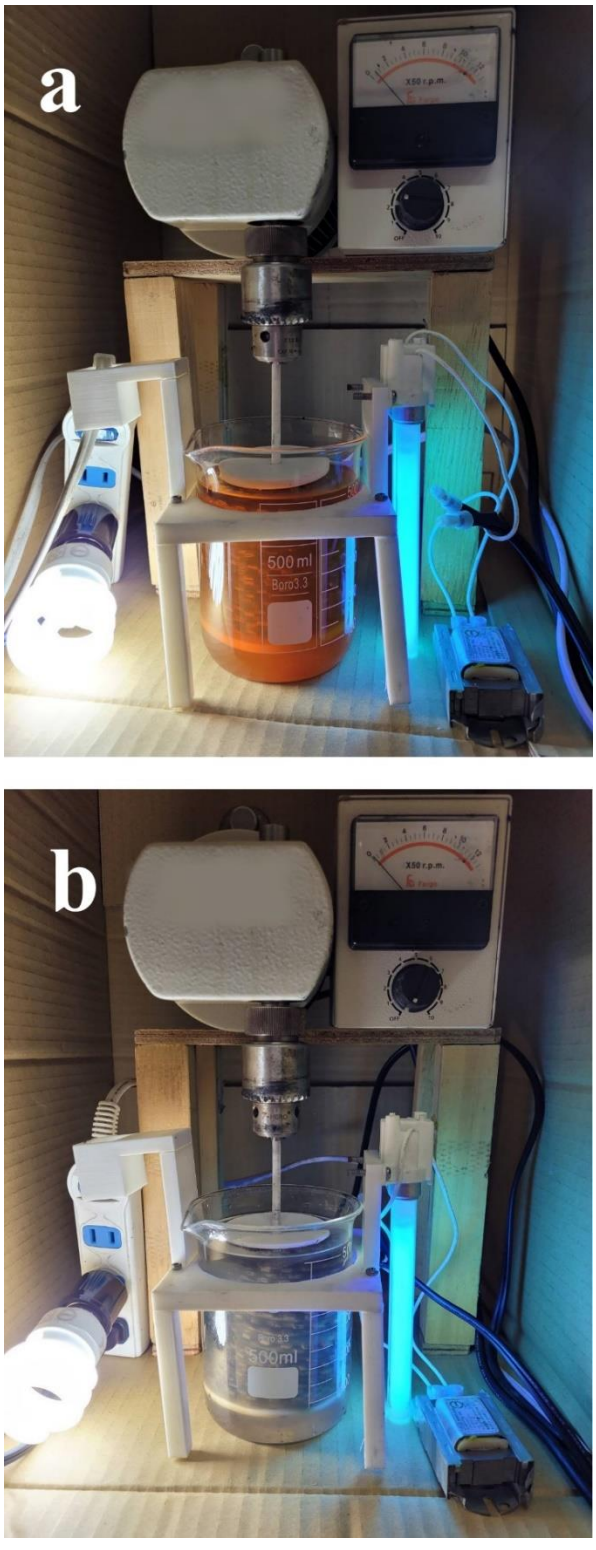

Fig.5-C.B. Lin et al.

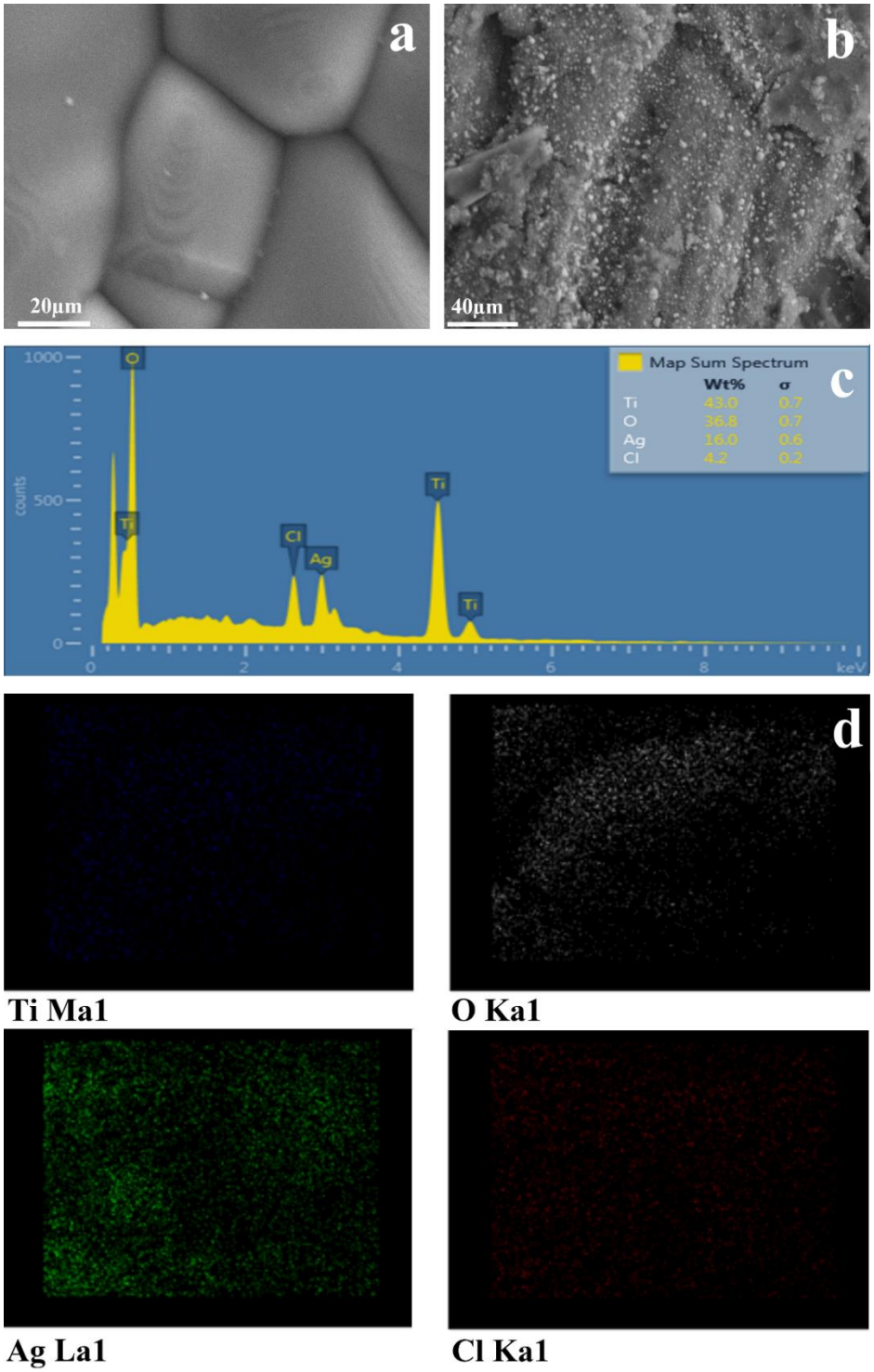

Fig.6-C.B. Lin et al.

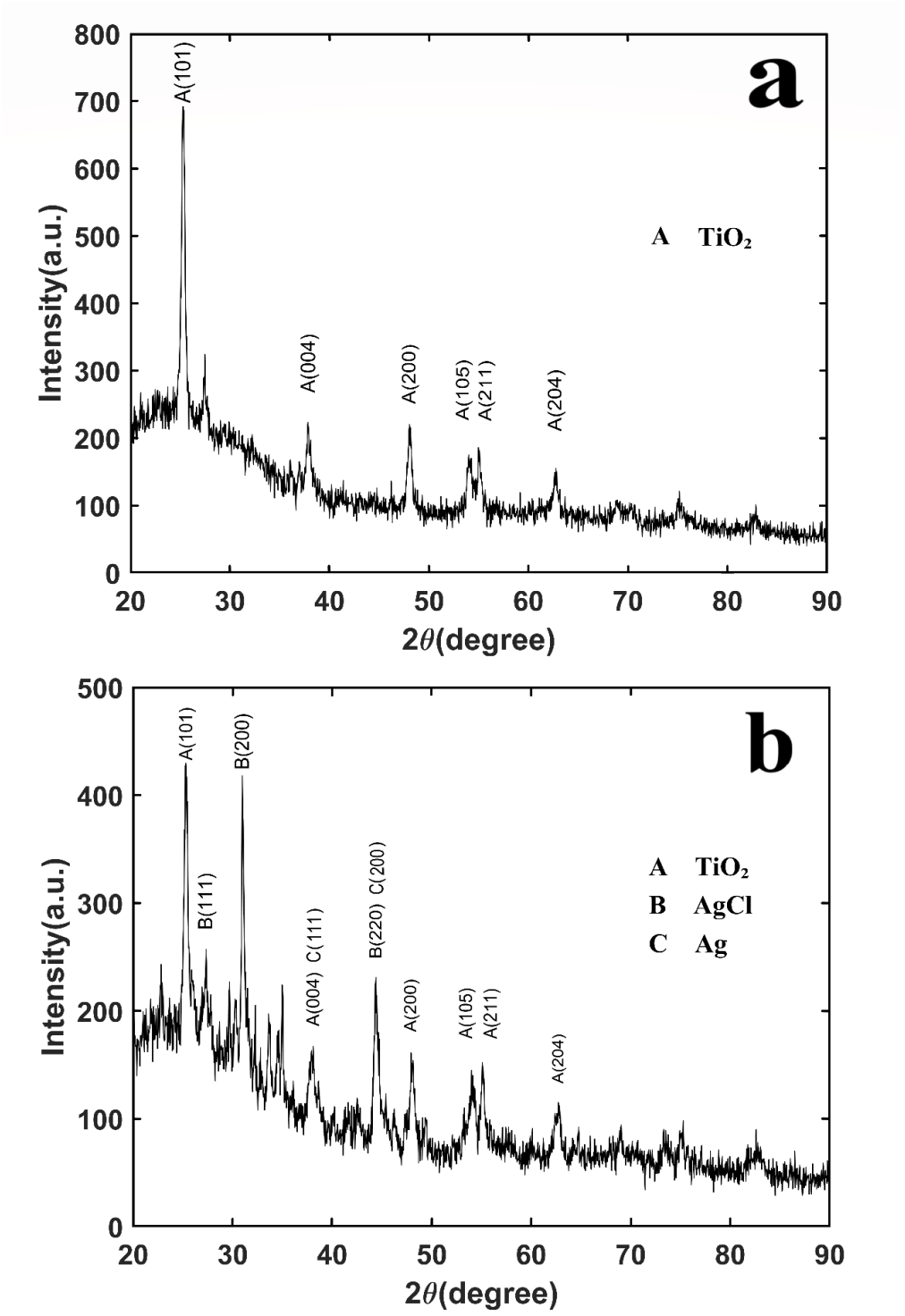

Fig.7-C.B. Lin et al.

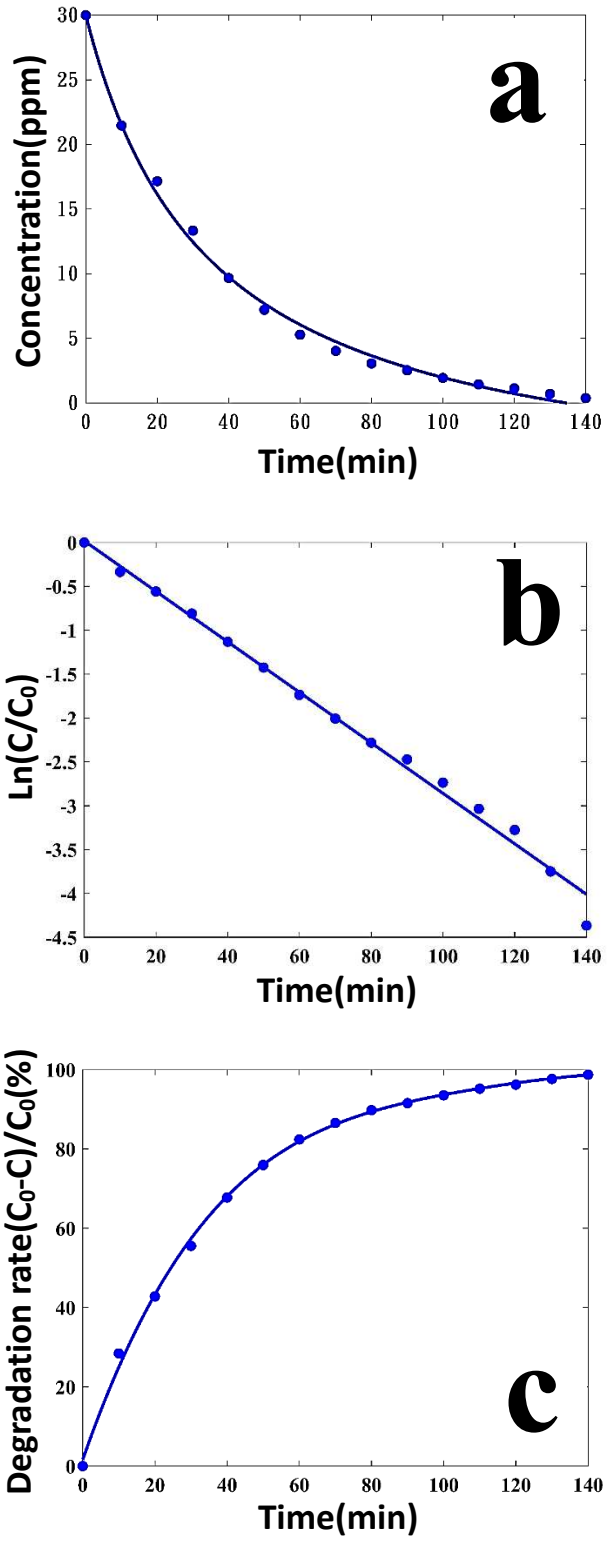

Fig.8-C.B. Lin et al.

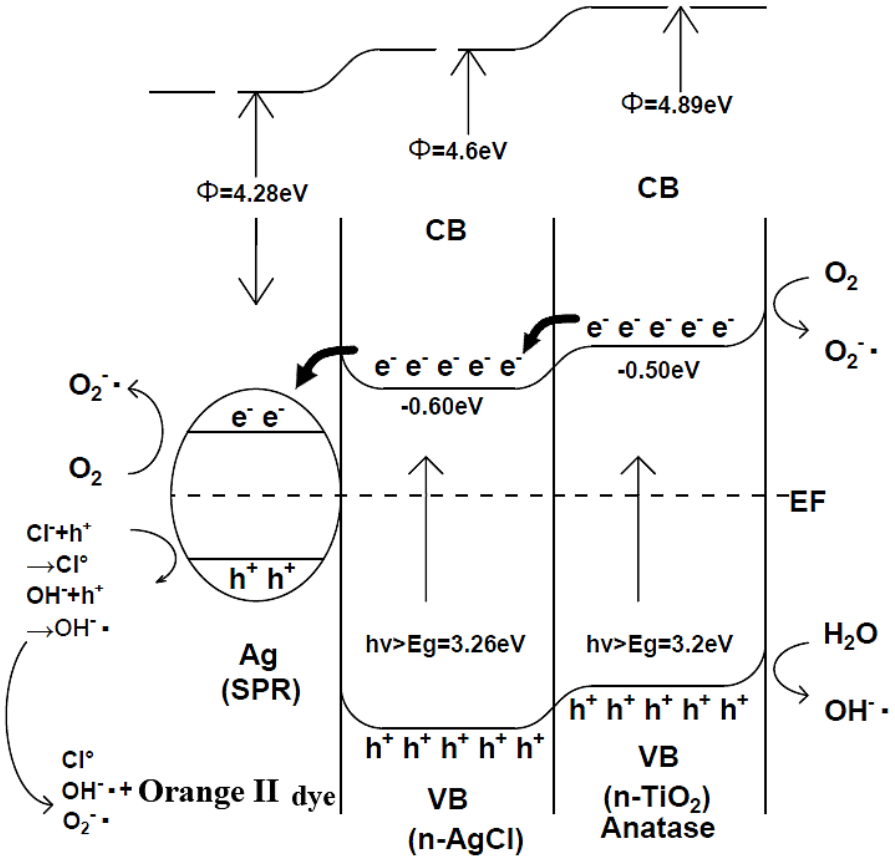

EF = Fermi energy level
VB = Valence band
CB = Conduction band

Fig.9-C.B. Lin et al.

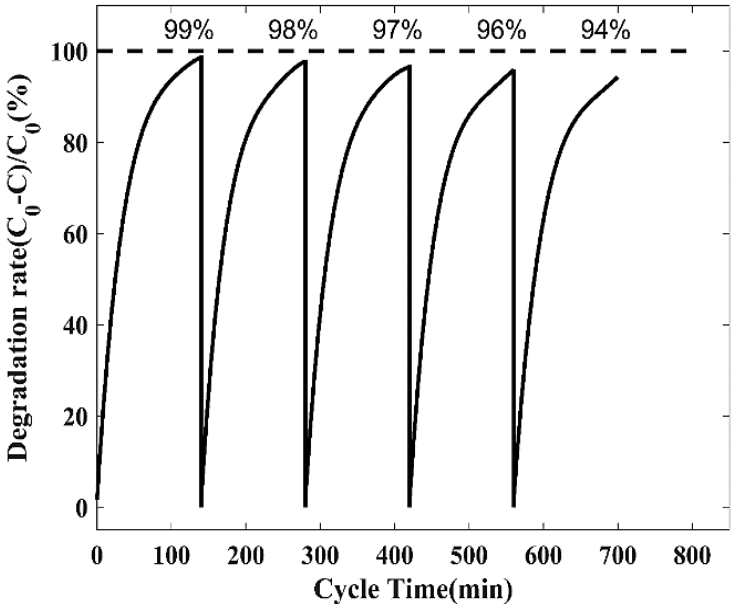

Fig.10-C.B. Lin et al.

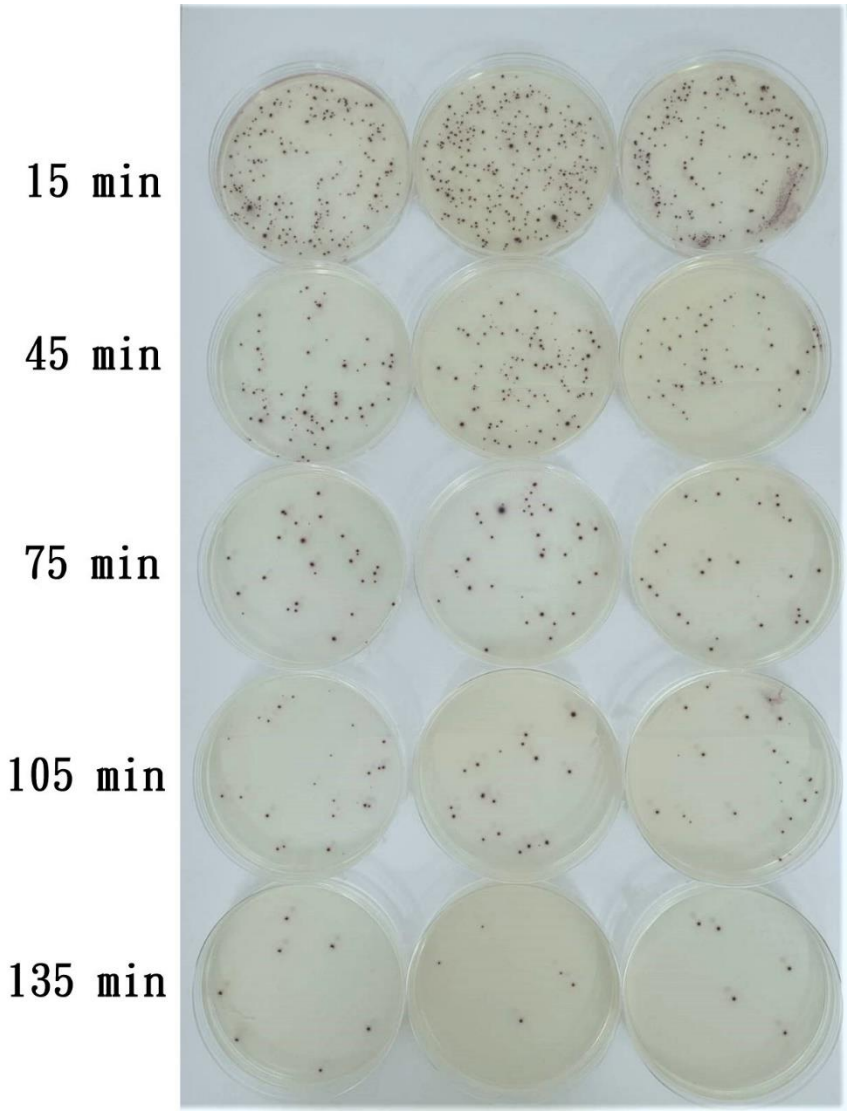

Fig.11-C.B. Lin et al.

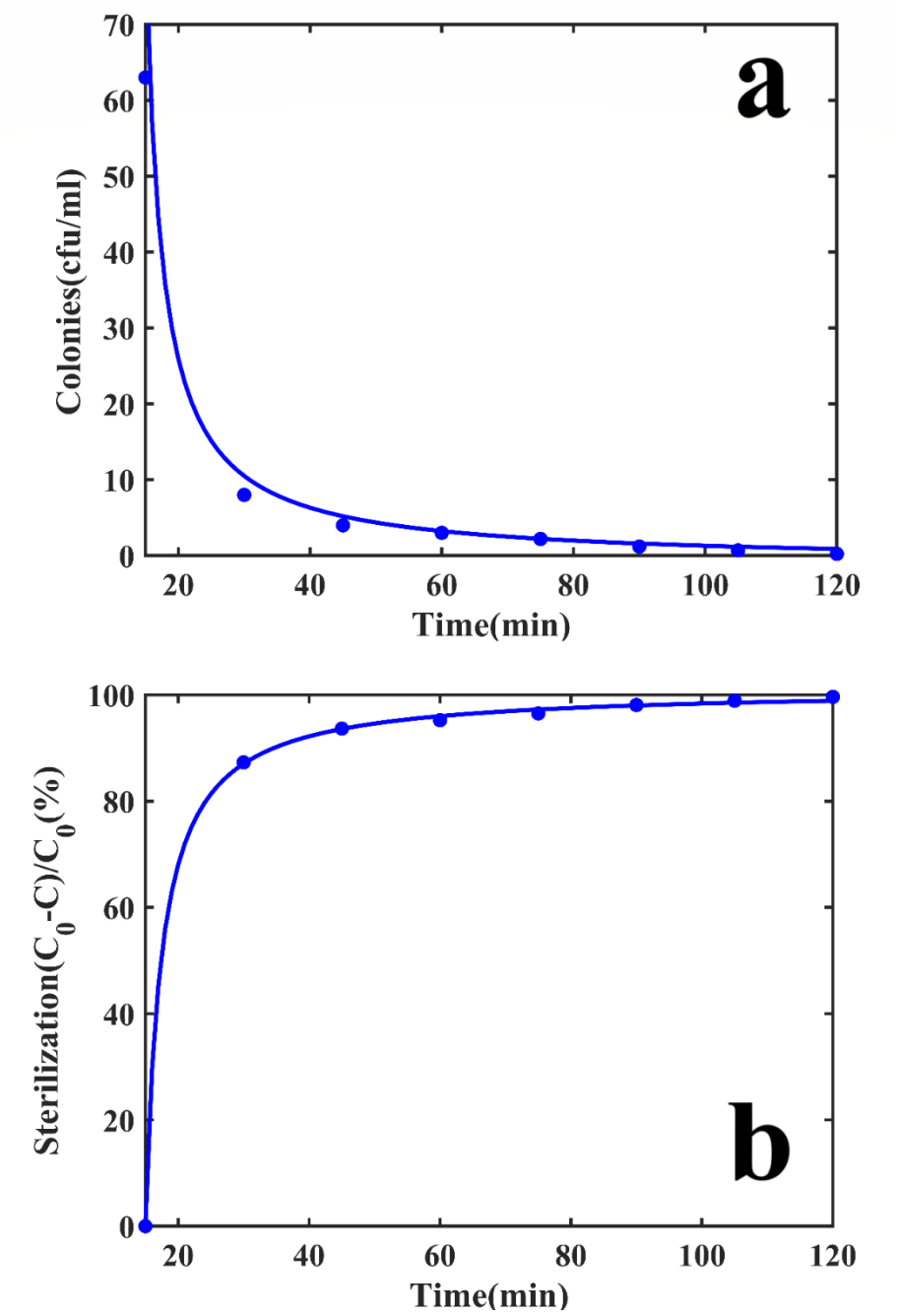

Fig.12-C.B. Lin et al.